

Directional Fluorescence Spectra of Laser Dye in Opal and Inverse Opal Photonic Crystals

Lydia Bechger,* Peter Lodahl, and Willem L. Vos[†]

Complex Photonic Systems (COPS), MESA⁺ Research Institute and Department of Science and Technology, University of Twente, P.O. Box 217, 7500 AE Enschede, The Netherlands

Received: June 10, 2004; In Final Form: March 22, 2005

We have investigated the fluorescence from R6G dye molecules embedded in fcc photonic crystals with a large range of lattice parameters. Both polystyrene opals and alumina inverse opals are studied, allowing us to compare direct and inverted structures. We observe clear stop bands in the fluorescence spectra, whose center positions, widths, and depths are analyzed and compared to stop bands from reflectivity measurements. In the frequency range of first-order stop gaps, the measured stop band centers and widths agree well with theoretical predictions. The depths are interpreted in terms of the mean free path (disorder) and the Bragg attenuation length (order). We observe intriguing enhanced emission at the blue side of the stop bands, which is attributed to the escape of diffuse light from the photonic crystal (related to both order and disorder). We perform the first experiments in the range of second-order stop gaps, which is the regime where the photonic band gap is anticipated. We observe complex multiple-Bragg features that correlate favorably with reflectivity peaks.

I. Introduction

Photonic crystals are three-dimensional dielectric structures with a periodicity comparable to the wavelength of light. Because of the periodic variation of the refractive index, the crystals possess unusual optical properties that affect the propagation and the emission of light. The main goal of the field is the achievement of a photonic band gap: a frequency range for which light cannot propagate in any direction because of Bragg diffraction.^{1,2} In the exciting case of a photonic band gap the emission by light sources in photonic crystals is completely inhibited.

The spontaneous emission of light sources embedded in photonic crystals can be strongly modified in either an angle-dependent or an angle-independent manner. Changes in the lifetime or in the total emitted power of sources are angle-independent effects. These effects are caused by a modified local density of states that depends sensitively on the emission wavelength and on the position of the source, but not on the emission direction.^{3–5} Inhibition of total emission was first reported in refs 6 and 7: titania inverse opals doped with laser dye showed a broadband 5-fold reduction of vacuum fluctuations. Recently, even control of the radiative lifetime of quantum dots in photonic crystals was demonstrated.⁸

In contrast, angle-dependent modification results from scattering of the emitted light that propagates through the complex anisotropic photonic crystal structure.⁹ In particular, Bragg diffraction by lattice planes is observed as a stop band in the emission spectrum.¹⁰ Such control of propagation plays a role in, e.g., laser action of dye in photonic materials.¹¹ Since a photonic band gap appears when stop bands are present in all directions simultaneously, it is essential to investigate the angle-dependent behavior of stop gaps. In this paper we discuss angle-dependent effects in emission experiments on dye-doped

polystyrene opals and inverse alumina opals. Inverted opals, consisting of interconnected air spheres in a solid semiconductor backbone (air-sphere crystals), have proven to be most effective photonic crystals.¹²

In general, Bragg resonances are characterized by three different quantities: the central position, width, and amplitude of the spectral feature. The spectral position, i.e., the center wavelength λ_c where the stop band appears, is determined by the lattice spacing and the average refractive index.¹³ Previously several groups determined the spectral position of the stop band. They embedded light sources like dye molecules,^{14–19} semiconductors,^{20,21} and rare earth ions^{22,23} in artificial and inverse opals and measured the modified emission.

An important quantity is the spectral width of the stop band $\Delta\lambda$, conveniently characterized by the full width at half-maximum (fwhm). The relative width ($\Delta\lambda/\lambda_c$) is proportional to the photonic interaction strength Ψ of a photonic crystal (see ref 24). An optimum for the relative width and therefore for the photonic strength was found as a function of the density of scatterers. The relative width is not only determined by photonic strength; also, disorder can contribute to broadening of the stop band. Nevertheless, careful reflectivity experiments have confirmed that such broadening can be made negligible (see ref 25).

The amplitude is the third characteristic feature and the least studied of all. Interestingly, photonic crystals can not only attenuate light emission but also enhance it. Megens et al.¹⁸ were the first to interpret attenuation of light emission in stop bands in optically thin crystals. They concluded that defects near the sample surface are crucial for the understanding of the limited attenuation. For optically thick crystals (thicker than a mean free path), Schriemer et al.¹⁹ proposed to describe the attenuation of light emission A as

$$A = 1 - \frac{l_{\text{Bragg}}}{l} \quad (1)$$

where l_{Bragg} is the Bragg length and l the mean free path of

[†] Also at Center for Nanophotonics, FOM Institute for Atomic and Molecular Physics, Kruislaan 407, 1098 SJ Amsterdam, The Netherlands. E-mail: w.l.vos@utwente.nl.

* Corresponding author. E-mail L.Bechger@tn.utwente.nl.

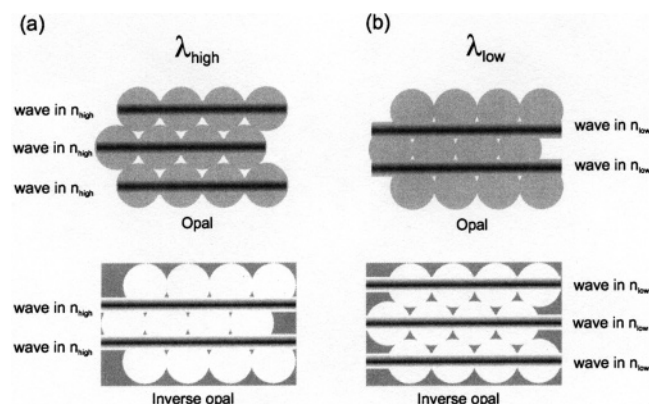


Figure 1. Schematic of the position of a standing wave in either an opal or an inverse opal. The standing waves are represented as horizontal gray bars. (a) At a certain wavelength λ_{high} the standing wave is mainly in the high index material n_{high} . This corresponds to a position in the opal at the equator and in the inverse opal at the pole. (b) At a wavelength λ_{low} the standing wave is mainly in n_{low} . Here the light is in the opal mainly at the poles and in the inverse opal mainly at the equator. Considering the position of the dye, at the equator, the pole, or evenly distributed, it can be concluded that the enhancement is not caused by standing wave effects.

light in the photonic crystal.²⁶ The Bragg length $l_{\text{Bragg}} = 2d_{hkl}/\pi\Psi$ is the distance that light can penetrate into a photonic crystal in the $[hkl]$ direction of a stop gap.²⁷ A short Bragg length is found for strongly photonic crystals since the light is strongly Bragg attenuated. The mean free path is the average distance light propagates before it is being diffused by disorder. The mean free path is inversely proportional to the concentration of scattering defects and their scattering cross section. For a constant mean free path stronger photonic crystals show more attenuation, since their Bragg length is shorter. Typical values of l_{Bragg}/l are between 0.2 and 0.5, corresponding to attenuations in the stop band of 50–80%.^{19,28}

While many experiments have demonstrated attenuation of emission, enhanced emission has never been reported in 3D photonic crystals. The ability to enhance emission in certain directions could become useful for creating efficient light sources. Theoretically, Galstyan et al.²⁹ have predicted enhancement near the edges of the stop bands. They proposed a model where standing wave effects determine enhancements either at the red part (λ_{high}) or at the blue side (λ_{low}) of the stop band (see Figure 1), similar to X-ray standing waves in condensed matter.³⁰ The effects are related to the well-known phenomenon that near a stop gap light is concentrated in the high index material at long wavelengths and in low index material at short wavelengths. In this paper we investigate emission from both polystyrene opals and inverse opals of alumina. In this way we are in an excellent position to compare direct and inverted structures and elucidate possible standing wave effects.

The photonic band gap for face-centered-cubic (fcc) crystals will occur in the wavelength range of the second-order Bragg diffraction. Here the density of states varies much more than at the first-order Bragg condition, and this provides a strong motivation for investigating emission from fcc crystals at higher order Bragg diffraction. The interaction between light and matter is stronger in these samples since light propagation is significantly influenced by more than one set of lattice planes. This results in a complex combination of several diffraction peaks, as opposed to first-order stop gaps. Previously, second-order reflectivity was observed from inverse titania opals,³¹ but emission from samples with a stop gap at second-order Bragg diffraction was never investigated. Here we present such a

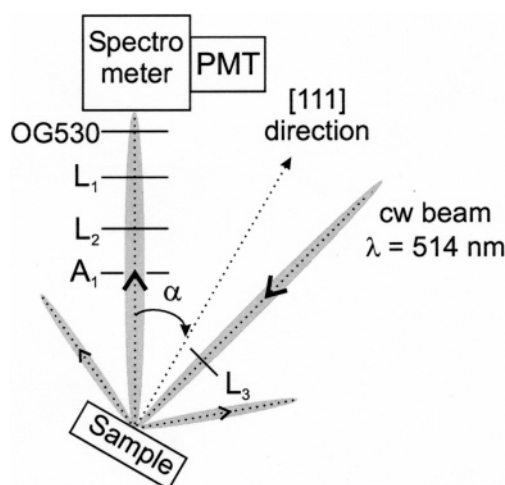


Figure 2. Schematic of the optical setup. An argon laser ($\lambda = 514$ nm) was focused on the (111) surface of the photonic crystal to excite the internal dye molecules. Part of the dye fluorescence of the excited light was collected in reflection at an angle α away from the surface normal. Lens L_3 was used to focus the pump beam on the sample, while L_2 and L_1 respectively collimated and focused the emitted light on the spectrometer. With aperture A_1 the angular spread of the emitted light could be adjusted. The photons were detected with a photomultiplier tube (PMT) via a prism spectrometer. The PMT was protected against direct reflected laser light by a 530 nm cutoff filter (OG530).

measurement using crystals with a lattice parameter tuned such that the second-order Bragg diffraction is in the emission range of our emission source.

In this paper, we investigate angle-dependent emission of Rhodamine 6G laser dye (R6G) in opals as well as inverse opals. Dyes are favorable since they exhibit broad emission spectra, are bleachable,¹⁸ and have high quantum efficiencies. We characterize stop bands by their center position, width, and amplitude. By comparing direct and inverse structures, we investigate standing wave effects. We explore photonic crystals with second-order Bragg diffraction using emission from internal light sources.

II. Experimental Section

The crystals were prepared via self-organization of colloidal polystyrene particles, followed by infiltration of the precursor of alumina. After calcination a high-quality inverse opal was produced. For more details about the preparation see also refs 32–34. The crystals, opals, and inverse opals were doped with laser dye, Rhodamine 6G, by soaking the crystal in a dilute ethanol solution (10^{-5} or 10^{-6} M). The concentration of the dye solution was kept low to prevent reabsorption of light and nonradiative transfer. The R6G molecules were absorbed either on the surface of the polystyrene spheres or on the inner surface of the backbone of the air spheres. The polystyrene opals consisted of nominally $r = 131 \pm 3$ nm spheres (denoted first-order samples) or $r = 238 \pm 2$ nm spheres (denoted second-order samples), as was measured with scanning electron microscopy (SEM). These radii were used in interpreting our measurements although the sample nomenclature follows the nominal values. The alumina inverse opals consisted of air spheres with $r = 169 \pm 3$ nm and were made from a polystyrene template with $r = 213$ nm.

The setup used to measure the emission spectra is displayed in Figure 2. The dye inside the crystal was excited with a continuous wave (CW) laser beam ($\lambda = 514$ nm, from a Lexel argon laser) with low power, i.e., less than 0.1 mW, to prevent bleaching of the dye and luminescence of polystyrene. The

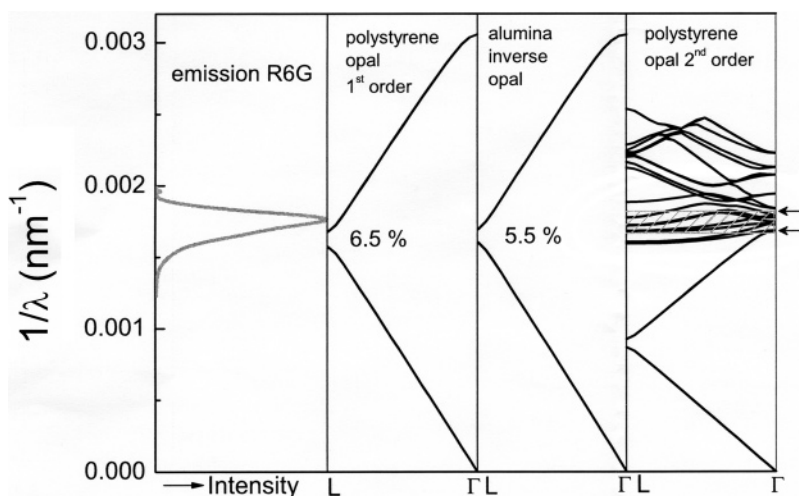


Figure 3. Emission of R6G compared with band structure calculations of the doped photonic crystals used in the experiments. The polystyrene opal with $r = 131$ nm has a stop gap width of 6.5%; the alumina inverse opal with $r = 169$ nm has a stop gap width of 5.5%. The polystyrene opal with $r = 238$ nm has a first-order stop gap in the infrared and a complex dispersion relation in the emission range of R6G. Consequently, a clear stop gap cannot be appointed; however, it is expected to appear in the hatched area between the arrows. The R6G spectrum displayed in this plot is taken from R6G dye adsorbed on a polystyrene opal with no Bragg attenuation in the emission range of R6G.

amount of bleaching at this power was negligible since there was no intensity drop after illuminating a particular spot for more than 4 h. The pump beam was focused with lens L_3 to a spot size of approximately $50 \mu\text{m}$ in cross section and impinged on the sample with an angle away from the Bragg angle to establish a sufficient penetration depth of the pump light into the crystal. The emitted fluorescence from the dye was collected at a detection angle α with respect to the normal of the (111) planes of the sample. If $\alpha = 0^\circ$, the surface of the crystal was perpendicular to the detection angle. Subsequently, the light was collimated with lens L_2 and focused with L_1 on the spectrometer slit. The aperture A_1 determined the angular spread of the collected light to $\pm 5^\circ$. The photons were detected by a photomultiplier tube (PMT) that was protected against direct reflected laser light by a color filter (OG530) placed in front of the Carl Leiss spectrometer. The OG530 filter cuts off the light below $\lambda = 530$ nm. Detector dark counts with typical values below 200 counts/s are obtained by averaging the signal obtained below 520 nm and are subtracted from each spectrum. The emission spectra were recorded between 503 and 815 nm. The slit widths of the spectrometer were set to 0.1 mm. With these settings a spectral resolution of ~ 4 nm was achieved.

To ensure only emission from internal light sources, the dye molecules on the outer surface were selectively bleached by illumination with an intense laser beam under the Bragg angle.¹⁸ The Bragg angle was determined by rotating the sample until the reflection was strongest. During bleaching the laser beam was not focused and roughly illuminated the whole sample. The power of the unfocused beam was 50 mW, yielding an intensity drop of a factor of 2 in half an hour. Reflectivity measurements were done on the same samples as in emission, with reflectivity methods outlined in ref 31. In the experiments, the beam size was about $500 \mu\text{m}$ in diameter on the sample.

III. Results

The frequencies of the stop gaps in the Γ - L direction³⁵ obtained from band structure calculations are plotted in Figure 3³⁶ and compared to the emission of R6G. From this graph it is clear that the first-order stop gaps of the polystyrene opal with $r = 131$ nm and the alumina inverse opal with $r = 169$ nm occur in the red part of the R6G emission spectrum. The expected stop gap widths are respectively 6.5 and 5.5%. The

first-order stop gap of the polystyrene opal with $r = 238$ nm appears in the infrared, but the second-order bands coincide well with the R6G emission spectrum. The second-order stop gap is quite complex³¹ and is placed between the 5th and 16th band, since the slope of these bands is comparable to the slope at low frequencies. The stop gap is marked with two arrows.

A.1. Emission of R6G in Opals with First-Order Stop Gap.

Emission spectra of R6G adsorbed in a polystyrene opal with $r = 131 \pm 3$ nm are displayed in Figure 4a. The spectra were collected at different detection angles and overlapped in the long wavelength limit (650 nm) where no photonic crystal effects are apparent. This is done to correct for the variations in detection efficiency at different angles. Correction factors for overlapping were always less than 2, and the $\alpha = 0^\circ$ spectrum was not scaled. From the spectra it is clear that the emission of R6G is suppressed over a wide spectral range. Especially the $\alpha = 0^\circ$ spectrum shows a strongly modified spectrum, i.e., suppression in a range from 575 to 625 nm. At a wavelength of 600 nm there is a clear attenuation. This wavelength is exactly at the position where the stop gap is expected on the basis of calculations using Bragg's law.¹³ With increasing angle the center position of the first-order Bragg diffraction shifts to shorter wavelengths. At $\alpha = 30^\circ$ the attenuation has moved to $\lambda = 575$ nm, and the emission starts to recover at the red part of the fluorescence spectrum. The $\alpha = 40^\circ$ spectrum is strongly modified at the blue part, and at the emission maximum of R6G ($\lambda = 550$ nm) the emission is intensely reduced. At $\alpha = 60^\circ$ the attenuation has moved past $\lambda = 500$ nm, and the R6G spectrum is unaffected as can be seen in Figure 4a.

To visualize the stop bands, the measured spectra are normalized to a carefully chosen reference sample: a polystyrene opal with a smaller lattice parameter. The stop band of this sample is at shorter wavelengths where R6G does not emit. Importantly, such a sample exhibits the same chemical properties as the photonic sample. The reference sample used for the normalization consisted of spheres of $r = 63$ nm and was doped with a similar dye concentration. The spectrum of this sample was measured at $\alpha = 0^\circ$ with a low power excitation source (a pulsed LED), and therefore scaling by a factor 8 was necessary. In Figure 4b the resulting intensity ratios of the spectra are displayed, which are scaled to unity in the long wavelength limit above 650 nm. The spectral position and width of the stop bands

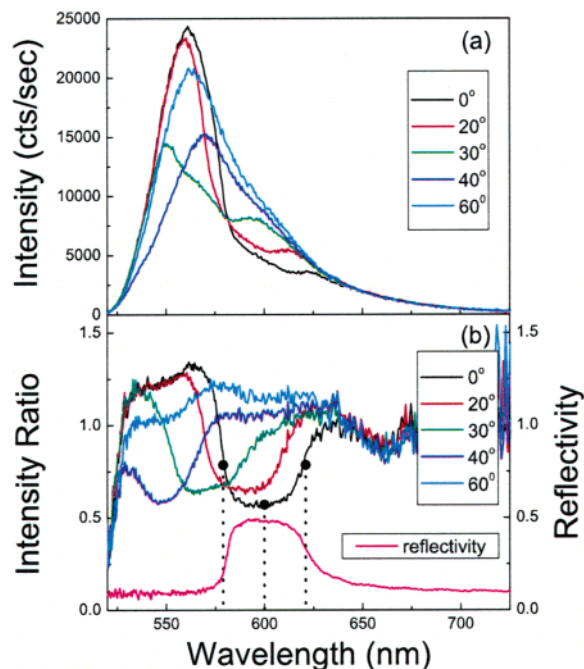


Figure 4. (a) Emission spectra of R6G adsorbed in a polystyrene opal with sphere size $r = 131$ nm. Black line represents $\alpha = 0^\circ$, red line $\alpha = 20^\circ$, green line $\alpha = 30^\circ$, blue line $\alpha = 40^\circ$, and the cyan line $\alpha = 60^\circ$. The $\alpha = 60^\circ$ spectrum is unaffected by the stop gap since the first-order Bragg diffraction is moved out of the emission spectrum of R6G. (b) Intensity ratios of the emission of R6G in a polystyrene opal with sphere size $r = 131$ nm. The spectra plotted in (a) are divided by the 0° spectrum of a $r = 63$ nm reference sample. The width and depth of the attenuation at $\alpha = 0^\circ$ are marked with black dots. The result of an external reflectivity measurement for $\alpha = 0^\circ$ is also included and shows an excellent match with stop bands from the emission experiment.

are clearly seen and shift toward the blue with increasing angle. At $\alpha = 0^\circ$ the center wavelength of the stop band is at 600 nm, as marked in the graph with a circle. The emission stop band is compared to complementary reflectivity measurements (in Figure 4b as a magenta line) performed with externally incident plane waves. The reflectivity peak of the polystyrene opal is as high as 50% and has the center position at $\lambda = 598$ nm, in excellent agreement with the position of the observed stop band measured in the emission experiments. It is clear that not only the position but also the shape of the stop band and the reflectivity peak match excellently.

The maximum attenuation in the stop band is 43%. Emission spectra taken at angles $\alpha = 20^\circ$, 30° , and 40° also show strong inhibition, with attenuations between 38 and 43%. These values are in good agreement with the 50% reflectivity measured with the external light source. Although the attenuations are intense, the emission does not completely disappear in the stop band. This will be discussed in more detail in the Discussion.

It is remarkable that there is an increase at the blue side of the spectrum; i.e., the intensity ratios are above unity in Figure 4b. For $\alpha = 0^\circ$ the intensity ratio reaches a value of 1.3 below $\lambda = 575$ nm. Similar results are observed for $\alpha = 20^\circ$ and 30° . The normalized spectrum taken at $\alpha = 40^\circ$ does not show this enhancement since the stop band has moved below $\lambda = 530$ nm where the color filter cuts off the light. The $\alpha = 60^\circ$ spectrum is more or less featureless. The strongly enhanced emission at the blue side of the stop band is observed here for the first time in 3D photonic crystals. It can be related to the diffuse propagation and internal refraction of the emitted light. This will be discussed further in the Discussion. The intensity

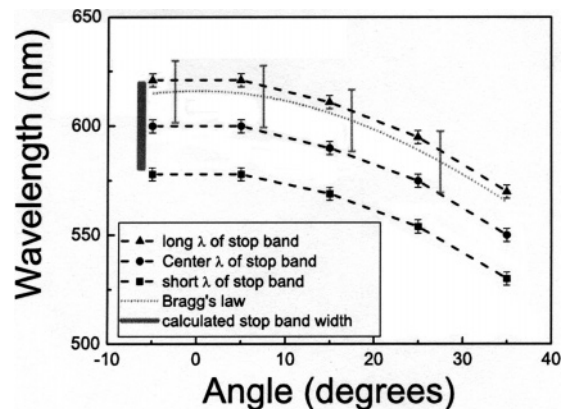


Figure 5. Wavelengths of the measured stop bands in a R6G-doped polystyrene opal with $r = 131$ nm as a function of detection angle. The center, upper, and lower edges of the stop band are denoted by circles, triangles, and squares, respectively. A comparison is made with Bragg's law where $n_{\text{avg}} = 1.44$ is used as average refractive index and internal refraction is taken into account. An excellent match is apparent between observed and calculated values.

ratio at $\alpha = 60^\circ$ is larger than unity in the range 575–625 nm and reaches a value of 1.2. For comparison, on titania inverse opals a large decrease in the intensity was observed for dye emission at $\alpha = 60^\circ$.⁶ This angle-independent effect was attributed to a modified density of states of the strongly photonic titania inverse opals. We do not observe a similar pronounced density of states effect for direct polystyrene opals, which is due to the lower refractive index contrast and difference in structure when comparing polystyrene opals to titania inverse opals.

The relative widths of the stop bands are an indication of the photonic strength of the crystal and can be deduced from Figure 4b by measuring the full width at half minimum. Two circles at $\lambda = 578$ and 621 nm mark the width in the $\alpha = 0^\circ$ spectrum in Figure 4b. The half-minimum appears at 0.79 at both sides. The relative width of the $\alpha = 0^\circ$ spectrum was found to be 7.2%. The relative widths of the stop bands at higher angles have comparable values between 7.1 and 7.2%. The relative width of the reflectivity peak is measured to be 6.9%, in complete agreement with the above values observed in the emission experiment. This agreement in relative widths is expected since the stop band in both reflectivity and emission experiments is determined by the outer crystal planes near the surface. Band structure calculations predict a relative stop gap width of 6.5%. This is slightly lower than observed in our experiments, and the minor discrepancy is due to the presence of unavoidable defects that are not taken into account in the calculations.

The half-minima and the center positions of the stop bands are plotted as a function of detection angle in Figure 5. This data set starts at -5° due to a small angular offset during alignment. The data are connected with lines. The relative width from band structure calculations is displayed as a vertical gray bar. As a comparison, the center position of the stop gap as predicted from first-order Bragg diffraction is plotted as the gray curve. The average refractive index is $n_{\text{avg}} = 1.44$, calculated with the known filling fraction ($\phi = 74\%$ v/v) and refractive index of polystyrene ($n_{\text{polystyrene}} = 1.59$) as a volume averaged index, which agrees within 0.7% with the Maxwell–Garnett average. Refraction of the light that exits the sample surface has been taken into account through Snell's law using n_{avg} . The assumed sphere size is the one that is measured with SEM, $r = 131$ nm. The SEM margin of ± 3 nm translates into a center

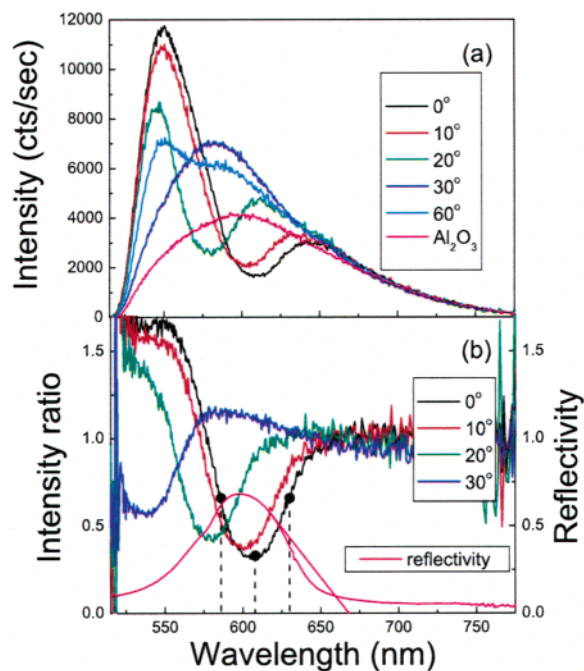


Figure 6. (a) Emission spectra of R6G adsorbed on the inner surfaces of an inverse opal of alumina. The air-sphere size is $r = 169$ nm. Attenuations in the emission of R6G are clearly seen over a wide range. The luminescence of bare alumina, measured from a nonphotonic air-sphere crystal, is represented by the magenta line. (b) Intensity ratios of the emission of R6G in an inverse alumina opal with sphere size $r = 169$ nm. The ratios are obtained by referencing the spectra in (a) to the 60° spectrum. The reflectivity peak measured at $\alpha = 0^\circ$ (magenta line) matches well with the position of the stop band.

position margin of ± 14 nm; thus, the theory agrees well with our experiments.

The measurement of stop bands from polystyrene opals with first-order Bragg was repeated on three samples, and all agreed well with each other regarding center position, relative width, and depth of the stop band.

B.2. Emission of R6G in Inverse Opals with First-Order Stop Gap. Figure 6a displays the emission spectrum of R6G in an alumina inverse opal with air-sphere size $r = 169 \pm 3$ nm. The spectra are collected at different detection angles and are overlapped in the long wavelength limit at 700 nm. The $\alpha = 30^\circ$ spectrum is not scaled. The emission is clearly reduced over a large wavelength range; especially the $\alpha = 0^\circ$ spectrum is suppressed over a wide spectral range reaching from 570 to 650 nm. With increasing angle the stop band shifts to shorter wavelengths. At $\alpha = 30^\circ$ the decrease in emission has moved to $\lambda = 550$ nm, and the red part of the R6G emission spectrum starts to recover. At $\alpha = 60^\circ$ the stop band has completely moved outside the emission region of R6G and results in an unaffected spectrum. The $\alpha = 60^\circ$ spectrum plotted in Figure 6a displays an extra hump at $\lambda = 590$ nm that is probably caused by alumina. The luminescence of the pure alumina backbone, measured on an undoped sample with same pump power, covers the range from 520 to 750 nm. The luminescence observed at long wavelengths (beyond 700 nm) seen in all the spectra is also due to luminescence of alumina. Importantly, the alumina luminescence does not influence the ability to extract stop bands since Bragg diffraction influences both the R6G emission and the alumina luminescence.

The alumina inverse opals clearly show more intense attenuation in the stop bands compared to the polystyrene opals. This can be seen in Figure 6b where the intensity ratios of the spectra are displayed. The spectra are divided by the 60° spectrum to

visualize the present stop bands,⁷ since a spectrum of a sample with a smaller lattice parameter was not available. The attenuations shift toward the blue with increasing angle. The maximum suppression for the $\alpha = 0^\circ$ spectrum is 67% compared to 43% for the polystyrene opals. The polystyrene opals have less photonic strength and hence a longer Bragg attenuation length than the alumina opals. We can estimate the expected attenuation in the experiment based on eq 1. The mean free path for polystyrene opals was measured to be $l \sim 15 \mu\text{m}$.²⁶ The mean free path of inverse opals was measured for titania and turned out to be $l \sim 15 \mu\text{m}$.²⁶ The alumina inverse opal exhibits the same structure factor as the titania inverse opal since it is also an air-sphere structure. Therefore, we can estimate l for alumina with the model of refs 26 and 37, where $l \propto 1/(m - 1)^2$. This yields a value of $l \sim 60 \mu\text{m}$ for alumina compared to $l \sim 15 \mu\text{m}$ for titania, since the mean free path is longer in a photonic crystal with a low index contrast, all structural parameters being equal.

Since $l_{\text{Bragg}} \propto 1/\Psi$ and $\Psi (= \Delta\lambda/\lambda_c)$ can be deduced from reflectivity measurements (not described here), the Bragg attenuation length is estimated to be $l_{\text{Bragg}} = 13 \mu\text{m}$. Taken together this results in an attenuation $A = 1 - 13/60 = 78\%$, in agreement with the observed attenuation of $\sim 67\%$. This agreement confirms our assumptions and demonstrates the simple models for l_{Bragg} , l , and eq 1 to be accurate.

The maximum attenuation in Figure 6b appears at $\lambda = 608$ nm (marked in the graph with a circle), and this position can be compared with reflectivity data taken from a similar sample made from a template with the same sphere size. The reflectivity peak of an inverse alumina opal with $r = 169$ nm is plotted in Figure 6b. The center position of the peak is at $\lambda = 598$ nm and slightly shifted, 10 nm, compared to the value observed in the emission measurements. As was concluded from detailed reflectivity measurements (not described here), this is not uncommon for the alumina inverse opals where on similar samples center positions were found varying from 558 to 613 nm. This variance is probably caused by differences in shrinkage during preparation resulting in smaller or larger air spheres, which is found even for crystals made from the same template.

Also on the inverse opals we observe enhancement at the blue side of the stop band. This increase is even larger than on the polystyrene opals and exceeds an intensity ratio of 1.5. It is interesting to remark that enhancement is found at the same spectral position relative to the stop band for both direct and inverted photonic crystals.

The relative widths of the stop bands are directly proportional to the photonic strength of the crystal. The fwhm is marked in Figure 6b, with two circles at wavelengths of 586 and 630 nm. The half-maximum is at 0.66 at both sides. The relative widths of the attenuations in the inverse alumina opals vary between 6.1 and 7.2%. These widths can be compared with the predicted value of 5.5%. The slight deviation from the measured value is possibly due to a mismatch in the filling fraction of alumina in the crystals and the filling fraction used for band structure calculations.

The relative width obtained in external reflectivity measurements is broader and gives a value of 10.4%. This deviation in width is attributed to the presence of disorder caused by different shrinkages. The shrinkage during calcination is $\sim 25\%$ and can vary throughout one sample, hence creating different sphere sizes in different areas. In the reflectivity measurements a wide beam is used and therefore many areas are averaged, and the differences in sphere sizes can cause broadening. On other alumina samples with similar sphere sizes relative widths of

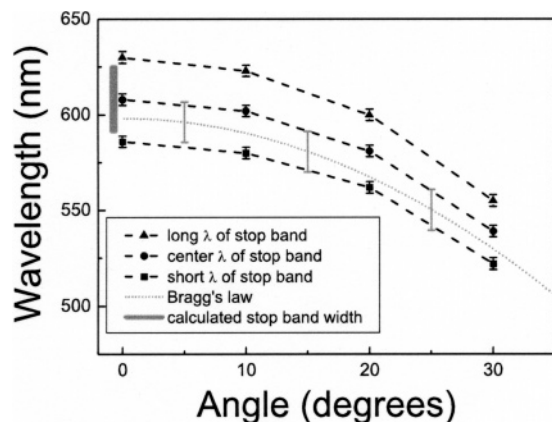


Figure 7. Angular dependence of the measured stop bands in a R6G doped inverse alumina opal with $r = 169$ nm. The positions of the center, upper, and lower wavelengths of the fwhm are plotted as a function of detection angle with respectively circles, triangles, and squares. A comparison is made with the center wavelength assuming single (111) Bragg diffraction, where $n_{\text{avg}} = 1.084$ is taken as average refractive index. Correction for internal refraction is done.

8.5% were found, i.e., close to the values observed in emission experiments.

In Figure 7 the angular dependency of the stop bands is displayed. The center, upper, and lower wavelength at half-height are plotted as a function of detection angle. The gray curve without symbols is the calculated center position assuming single (111) Bragg diffraction; the width of this calculated stop gap is plotted as a vertical gray bar just below $\alpha = 0^\circ$. The average refractive index is estimated as $n_{\text{avg}} = 1.084$, from an estimated filling fraction of $\phi \sim 11\%$ and the refractive index of alumina, $n_{\text{alumina}} = 1.76$. The curve of the calculated stop gap starts at a slightly lower value, i.e., at $\lambda = 598$ nm compared to 608 nm for the measured wavelength. This can be caused by a difference in sphere size since the sphere size is determined by measuring air spheres with an electron micrograph. For the alumina air spheres that were measured on a similar sample as the sample used for the emission measurements, a deviation in sphere size of ± 3 nm was found in the SEM measurement. Such a variation can cause a shift in center wavelength of ± 10 nm, which agrees well with the measured value. This variation is indicated in Figure 7 as error bars on the curve of Bragg's law and matches very well with the measured value.

C.3. Emission of R6G in Opals with Second-Order Bragg Stop Gap. In Figure 8a the emission spectra of R6G in a polystyrene opal with $r = 238 \pm 2$ nm are displayed. To allow subsequent intensity normalization, the spectra are overlapped at λ chosen at 660 nm (the $\alpha = 20^\circ$ spectrum is not scaled). This wavelength is chosen since band structure calculations revealed that the density of states in this range closely resembles the free space value. It can be seen in Figure 8a that the emission of R6G is modified over a wide range reaching from 625 to 570 nm, which is almost the complete emission range of R6G. Particularly the $\alpha = 0^\circ$ spectrum shows a strongly altered emission with a large decrease at $\lambda = 598$ nm. Also at the peak emission, $\lambda = 562$ nm, clear suppression is observed. At the blue side of the emission spectrum, around $\lambda = 550$ nm, the intensity is reduced as well. This is clearly different from the first-order samples where no decrease in emission was observed below wavelengths of 560 nm. With increasing angle the inhibition of emission becomes less, resulting in an increase in intensity at all wavelengths compared to the $\alpha = 0^\circ$ spectrum. In the $\alpha = 15^\circ$ spectrum the attenuations that are seen in the $\alpha = 0^\circ$ spectrum have slightly

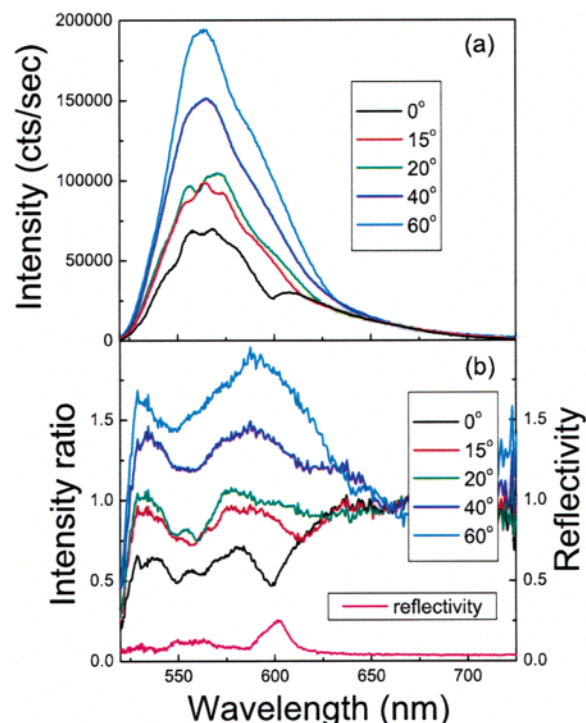


Figure 8. (a) Emission spectra of R6G adsorbed in a polystyrene opal with sphere size $r = 238$ nm. The second-order Bragg diffraction of this sample coincides with the emission range of R6G. (b) Intensity ratios obtained by referencing the spectra plotted in (a) to a polystyrene opal with a smaller sphere size ($r = 63$ nm). The position as well as the shape of the reflectivity peak matches excellently with the attenuation at $\alpha = 0^\circ$.

moved toward the blue. At $\alpha = 20^\circ$ the emission at the red part of the R6G spectrum partly recovers. A narrow attenuation is observed at $\lambda = 560$ nm. Beyond $\alpha = 20^\circ$ the sharp attenuations are not visible anymore. Obviously, the attenuations do not simply shift with $\cos \alpha$ as seen in experiments with first-order samples.

To highlight the stop band features in the spectra, we divide the spectra of Figure 8a by the spectrum of a reference sample with a sphere size of $r = 63$ nm. The Bragg diffraction of this reference sample appears far below $\lambda = 300$ nm and therefore will not influence the R6G emission spectrum. The resulting intensity ratios are plotted in Figure 8b and show strong modulations over the whole emission range of R6G. The intensity ratio of the $\alpha = 0^\circ$ spectrum shows a strong suppression from 625 to 525 nm. At $\lambda = 598$ nm, corresponding to a reduced frequency a/λ of 1.12, the emission is attenuated by 53%. This attenuation has a sharp triangular shape at $\lambda = 600$ nm. Two less intense attenuations are observed at a wavelength of 562 and 550 nm ($a/\lambda = 1.22$); here the emission is decreased with respectively 52 and 46%. In the $\alpha = 15^\circ$ spectrum the attenuations that are seen in the $\alpha = 0^\circ$ spectrum have slightly moved, ~ 7 nm, toward the blue. The attenuations appear at wavelengths 569 and 556 nm compared to 562 and 550 nm in the $\alpha = 0^\circ$ spectrum. The $\alpha = 40^\circ$ and 60° spectra are not attenuated, but rather enhanced. The $\alpha = 40^\circ$ spectrum has a maximum value of 1.45 at $\lambda = 585$ nm whereas the $\alpha = 60^\circ$ spectrum increases to as much as 1.9 at this wavelength. The features in the $\alpha = 40^\circ$ and 60° spectra are very similar: at $\lambda = 585$ nm an intense enhancement and at $\lambda = 550$ nm a strong attenuation.

For comparison, the reflectivity of a similar sample with same sphere size is plotted in Figure 8b. The reflectivity ratio is scaled with a factor 3 for clarity. It can be seen that the center position

of the main reflectivity peak coincides perfectly, within 3 nm, with the position of the sharp triangular attenuation in the 0° spectrum. The reflectivity signal observed between 570 and 545 nm is not distinguishable in separate peaks, but the position matches well with the observed attenuations in the emission spectrum. In recent reflectivity experiments on thin opal films by Galisteo-Lopez et al.,³⁸ one reflectivity peak has been observed at reduced frequencies $a/\lambda = 1.1$ and a double peak at 1.2. The occurrence of these features agrees with our reflectivity data. Interestingly, the shapes and positions of these three reflectivity peaks correlate very well with our increased attenuation bands.

The first interpretation of second-order diffraction features in fcc photonic crystals was carried out by Vos and van Driel.³¹ They studied second-order Bragg diffraction of titania inverse opals with angle-resolved reflectivity and compared their results with band structure calculations: as opposed to simple Bragg diffraction for first-order samples, light Bragg diffracts from many lattice plane simultaneously in second-order samples. This results in spectral positions of stop gaps that hardly vary with detection angle. Indeed, in our emission experiments the spectral position of the measured stop bands change moderately with angle; from $\alpha = 0^\circ$ to $\alpha = 40^\circ$ nearly the complete emission spectrum of R6G ranging from 525 to 625 nm is modified. This angle-independent width is supplementary evidence for the strong photonic character of these second-order polystyrene opals. In two recent papers, it has been proposed that the complex transmission or reflectivity features in opals at high frequencies are due to a decreased coupling of light to light modes with a low dispersion.^{38,39} Recently, in near-field optical experiments Flück et al. investigated the coupling of light into opal photonic crystals, and they observed intricate spatial patterns that shift with frequency due to the presence of the second-order stop band.⁴⁰

It is clear that the shape of the modified emission spectra of R6G is completely different from the modified emission spectra of R6G in polystyrene opals with first-order Bragg diffraction. In second-order Bragg diffraction a series of attenuations at several wavelengths are seen, as opposed to the clear single stop band in first-order Bragg diffraction. This difference can clearly be seen in the photonic band structures where the first-order gap of the $r = 238$ nm sample in the $\Gamma-L$ direction shows one clear stop gap (see Figure 3). The second-order Bragg diffraction, however, that appears at shorter wavelengths is a complex sum of band structures that do not form a single gap. We expect the stop gap to be between the 5th and 16th band since these bands have slopes similar to the dispersion of a homogeneous medium with an index equal to the average refractive index. This interpretation has recently also been taken by ref 38. In Figure 3 this area is hatched and marked with two arrows.

The attenuation observed in these second-order Bragg samples is larger (53%) than the attenuation found in the first-order samples where the maximum attenuation was found to be 43%. If we assume the mean free path in opals to be the same for first- and second-order opals,²⁶ we find that the Bragg length is shorter for the second-order opal (see also eq 1). This is consistent with the width of the attenuated emission, which is much broader for the second-order Bragg diffraction, and thus indicates a larger photonic strength.

It can be speculated whether the features at $\lambda = 600$, 562, and 550 nm in Figure 8 are a result of surface grating modes as was first explored in 2D photonic crystals by Labilloy et al.⁴¹ These grating modes can influence the optical properties of the

photonic crystal and should therefore be examined before excluding them. For our fcc-packed crystals the longest grating spacing d is given by $d = (3/8)^{1/2}a_{\text{fcc}}$, where a_{fcc} is the known lattice parameter. For the polystyrene opals with radius 238 nm the first-order grating mode appears at maximum 412 nm. This is far to the blue compared to the emission range we explored. Therefore, grating modes can be excluded.

We have observed that the shape and position of the attenuations change with increasing detection angle and cannot be explained by simple Bragg diffraction. Since the band structure calculations already showed a complex collection of bands and not a distinct stop gap, it is a challenge to interpret the observed features. It is clear that further theoretical interpretation in this area is necessary and an important subject for further research. Our experiments on emission from photonic crystals with second-order Bragg diffraction are a first step to elucidate emission in the case of a photonic band gap, since for fcc crystals the photonic band gap will appear at this second-order Bragg. This again illustrates the importance of investigating higher order Bragg diffraction.

IV. Discussion: Enhanced and Attenuated Fluorescence

A remarkable feature in the observed intensity ratios is the increase in emission at the blue side of the spectrum; i.e., there is more emission at shorter wavelengths in a given direction than is expected on the basis of the emission properties of R6G. This increase in intensity is seen in both first-order samples; the polystyrene opal with $r = 131$ nm and the alumina inverse opal with $r = 169$ nm. For the polystyrene opal the enhancement can be seen in the $\alpha = 0^\circ$ spectrum in Figure 4b. The wavelength region over which the emission is attenuated ranges from 575 to 625 nm. Below $\lambda = 575$ nm, however, the intensity ratio exceeds unity and reaches a value of 1.3. In the alumina inverse opals (see Figure 6b), an enhancement of 1.6 is observed. This phenomenon can be explained with the so-called escape function of diffuse light, a model developed by ref 28. In essence, if transport of light in certain directions is limited due to internal Bragg diffraction, the chance of escaping in the other existing angles is enhanced. Previously enhancement effects were observed in angle-resolved transmission experiments with external light beams;^{28,37} however, we report here for the first time enhancement of internal light sources. It appears that in real photonic crystals light is multiply scattered due to unavoidable disorder. Exactly this diffuse light transport can theoretically explain the enhancement. We expect disorder present in the samples used in our emission experiments to cause similar phenomena as in the transmission experiments; since the emission of R6G in certain directions is suppressed due to internal Bragg diffraction, the R6G emission in other directions is increased. In our experiments the enhancement is seen in both direct opal and indirect inverse opal structures at the blue side of the stop band.

As discussed above, one proposed mechanism for enhanced emission was the formation of standing waves at the edges of stop gaps.²⁹ However, we argue that standing waves cannot be responsible for the enhancement reported here. Figure 1 shows a schematic of standing waves in either n_{high} or n_{low} . At wavelengths λ_{high} and λ_{low} the standing wave is respectively mainly in the high index material n_{high} and in the low index material n_{low} . At λ_{high} this corresponds to a position in the opal at the equator and in the inverse opal at the pole. At wavelength λ_{low} the light is in the opal mainly at the poles and in the inverse opal mainly at the equator. If we then make three assumptions considering the position of the adsorbed dye molecules, it can

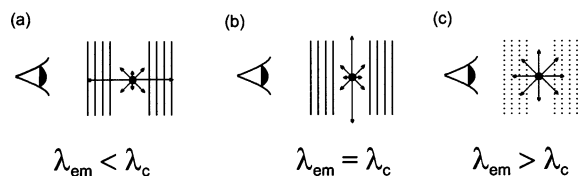


Figure 9. Cartoon of a light source emitting at constant wavelength λ_{em} in photonic crystals with one set of crystal planes. (a) Light is emitted at a wavelength λ_{em} below the stop band wavelength (λ_c). The light can be diffracted from the lattice planes, and light can be inhibited and enhanced in certain directions. (b) The emission is in the stop band wavelength, $\lambda_{em} = \lambda_c$. Inhibition takes place, and therefore enhancement can occur in other directions. (c) If light is emitted with a wavelength longer than λ_c , the light will not experience Bragg diffraction and no enhancement and attenuation are observed.

be ruled out that the enhancement is caused by standing wave effects. (1) If dye is mostly present at the poles, enhancement would be observed for opals at the blue wavelength (λ_{low}) and for inverse opals at the red wavelength side (λ_{high}) of the stop gap. (2) If the dye is mostly present at the equator, enhancement would be observed for opals at the red wavelength (λ_{high}) and for inverse opals at the blue wavelength side (λ_{low}) of the stop gap. (3) Assuming the dye is evenly distributed on the surface of the spheres, it is not immediately obvious at which wavelength enhancement occurs. Still, if an opal would show enhancement at the blue side, an inverse opal will then show enhancement at the red side. Or conversely, if the opal enhances at the red side, the inverse opal has enhancement at the blue side. In any case, we observe the enhancement only at the blue side of the stop gap for both direct and inverse opals, in disagreement with all three scenarios above. Therefore, we rule out that the enhancement is caused by standing wave effects.

Why enhancement is only present at the blue side of the 0° stop gap can be schematically illustrated with Figure 9. A light source in a photonic crystal is emitting at λ_{em} . Note that the light is diffuse in the bulk of the sample. When light is emitted at a wavelength in the stop band wavelength ($\lambda_{em} = \lambda_c$), it is diffracted from lattice planes and less light is detected at $\alpha = 0^\circ$. The diffracted light has a higher probability to escape at other angles, causing enhancement at certain wavelengths. When the stop band wavelength is shifted toward longer wavelengths ($\lambda_{em} < \lambda_c$), the emitted light λ_{em} is not Bragg diffracted from lattice planes at $\alpha = 0^\circ$ but encounters Bragg diffraction at higher angles. Because of the Bragg attenuation at these high angles, more light is detected in the allowed directions, e.g., $\alpha = 0^\circ$. When the stop band wavelength is shifted toward a shorter wavelength ($\lambda_{em} > \lambda_c$), however, the emitted light λ_{em} will not experience internal diffraction, also not at higher angles, and no enhancement will be observed. These three situations for one and the same angle (e.g., $\alpha = 0^\circ$) are exactly what is observed in the data in Figures 4b and 6b.

To investigate the enhancements of the alumina inverse opals and the polystyrene opals, we compared the amount of attenuation and enhancement as a function of angle (see Figures 10 and 11). The internal angles are displayed at the top x -axis. In Figure 10 the intensity ratios of the first-order polystyrene opal are displayed (cf. Figure 5). The attenuations are slightly above 0.50, and the enhancements are at ~ 1.25 . The attenuations and enhancements are more or less constant with angle. In Figure 11, the intensity ratios of the inverse alumina sample are displayed, and correlation between enhancement and attenuation is more pronounced, i.e., large enhancement correlations with strong attenuation. In the $\alpha = 0^\circ$ spectrum of the alumina inverse

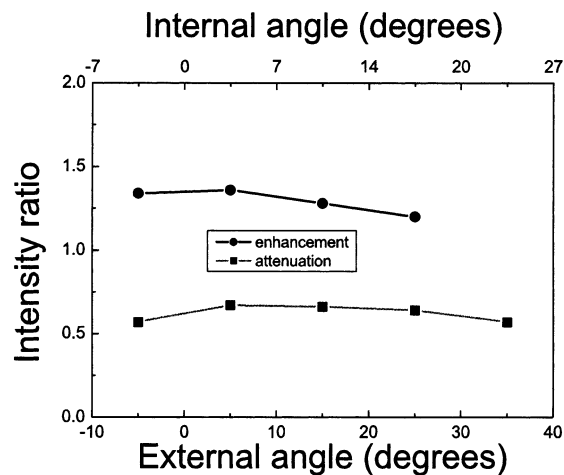


Figure 10. Intensity ratios of the attenuations and enhancements of the first-order polystyrene opal plotted as a function of angle. The lines are guides to the eye. At $\alpha = 40^\circ$ the data point for enhancement is missing since here the light is cut off by the filter. Error bars are comparable to the symbol size.

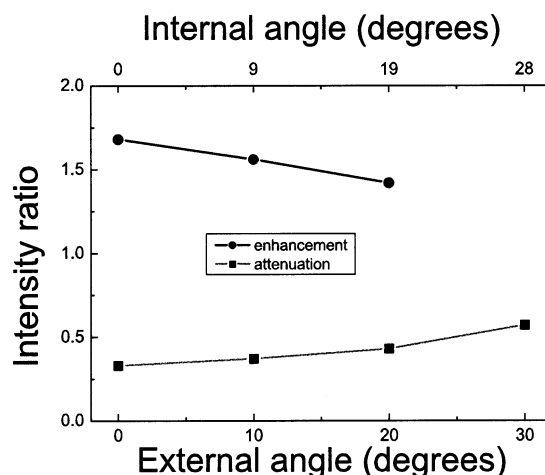


Figure 11. Intensity ratios of observed attenuations and enhancements in an alumina inverse opal. Strong angle-dependent behavior is apparent where the amount of enhancement and attenuation decrease with angle. An intensity ratio for the enhancement at $\alpha = 30^\circ$ is lacking since the light is cut off by a color filter.

opal, the intensity ratio is below 0.40 and the enhancement is 1.6. A larger variation is seen in the attenuations and enhancements as a function of angle. Here it is clearly seen that with increasing angle the attenuation decreases and also the enhancement lowers. The changes of these spectral features are expected at the same internal angles. Since the opals have a higher average refractive index than the inverse opals, the changes occur at smaller external angles for the inverse opals and are therefore more obvious (see Figure 11). The resulting difference in behavior between the opals and inverse opals is clear from a comparison of Figures 10 and 11. From these figures, it is also apparent that the observed enhancement is angle-dependent, in agreement with ref 28.

V. Conclusions

We have shown that the polystyrene opals and alumina inverse opals are efficient photonic crystals. The attenuations seen in the direct and indirect structures could be well explained with different mean free paths and Bragg attenuation lengths. We are the first to explore emission experiments with second-order photonic crystals and demonstrated strongly modified

emission spectra from these crystals. The first-order samples, opals as well as inverse opals, displayed strongly attenuated emission as well as increased emission at the blue side of the stop band. This enhancement was qualitatively explained with the escape of diffuse light. The enhancement observed and explained in our experiments was the first measured with internal sources. The widths of the measured stop bands show values that agree well with widths observed in reflectivity measurements and theory. Since the quantum efficiency of the emitters is in these samples, the photonic systems investigated here are very promising for time-resolved measurements, which will be our next research goal.

Acknowledgment. We thank Femius Koenderink for assistance and useful discussions, Eliane Flück and Ivan Nikolaev for experimental help, and Ad Lagendijk for encouragement and support. This work is part of the research program of the Stichting voor Fundamenteel Onderzoek der Materie (FOM), which is financially supported by the Nederlandse Organisatie voor Wetenschappelijk Onderzoek (NWO).

References and Notes

- (1) Yablonovitch, E. *Phys. Rev. Lett.* **1987**, *58*, 2059.
- (2) John, S. *Phys. Rev. Lett.* **1987**, *58*, 2486.
- (3) Suzuki, T.; Yu, P. K. L. *J. Opt. Soc. Am. B* **1995**, *12*, 570.
- (4) Sprik, R.; van Tiggelen, B. A.; Lagendijk, A. *Europhys. Lett.* **1996**, *35*, 265.
- (5) Vats, N.; John, S.; Busch, K. *Phys. Rev. A* **2002**, *65*, 043808.
- (6) Koenderink, A. F.; Bechger, L.; Schriemer, H. P.; Lagendijk, A.; Vos, W. L. *Phys. Rev. Lett.* **2002**, *88*, 143903.
- (7) Koenderink, A. F.; Bechger, L.; Lagendijk, A.; Vos, W. L. *Phys. Status Solidi A* **2003**, *197*, 648.
- (8) Lodahl, P.; van Driel, A. F.; Nikolaev, I. S.; Irman, A.; Overgaag, K.; Vanmaekelbergh, D.; Vos, W. L. *Nature (London)* **2004**, *430*, 654.
- (9) P. St. Russell, J.; Birks, T. A.; Lloyd-Lucas, F. D. In *Confined Electrons and Photons*; Burstein, E., Weisbuch, C., Eds.; Plenum: New York, 1995; pp 585–633.
- (10) Stop bands in experimental spectra (emission or reflectivity) usually correspond to stop gaps in the dispersion relation.
- (11) Shibaev, P. V.; Kopp, V. I.; Genack, A. Z. *J. Phys. Chem. B* **2003**, *107*, 6961.
- (12) López, C. *Adv. Mater.* **2003**, *15*, 1679.
- (13) Vos, W. L.; Sprik, R.; van Blaaderen, A.; Imhof, A.; Lagendijk, A.; Wegdam, G. H. *Phys. Rev. B* **1996**, *53*, 16231.
- (14) Bogomolov, V. N.; Gaponenko, S. V.; Germanenko, I. N.; Kapitonov, A. M.; Petrov, E. P.; Gaponenko, N. V.; Prokofiev, A. V.; Ponyavina, A. N.; Silvanovich, N. I.; Samoilovich, S. M. *Phys. Rev. E* **1997**, *55*, 7619.
- (15) Yamasaki, T.; Tsutsui, T. *Appl. Phys. Lett.* **1998**, *72*, 1957.
- (16) Yoshino, K.; Lee, S. B.; Tatsuhara, S.; Kawagishi, Y.; Ozaki, M.; Zakhidov, A. A. *Appl. Phys. Lett.* **1998**, *73*, 3506.
- (17) Romanov, S. G.; Maka, T.; Torres, C. M. S.; Muller, M.; Zentel, R. *Appl. Phys. Lett.* **1999**, *75*, 1057.
- (18) Megens, M.; Wijnhoven, J. E. G. J.; Lagendijk, A.; Vos, W. L. *J. Opt. Soc. Am. B* **1999**, *16*, 1403.
- (19) Schriemer, H. P.; van Driel, H. M.; Koenderink, A. F.; Vos, W. L. *Phys. Rev. A* **2001**, *63*, 011801.
- (20) Blanco, A.; López, C.; Mayoral, R.; Míguez, H.; Meseguer, F.; Mifsud, A.; Herrero, J. *Appl. Phys. Lett.* **1998**, *73*, 1781.
- (21) Lin, Y.; Zhang, J.; Sargent, E. H.; Kumacheva, E. *Appl. Phys. Lett.* **2002**, *81*, 3134.
- (22) Romanov, S. G.; Fokin, A. V.; De La Rue, R. M. *Appl. Phys. Lett.* **2000**, *76*, 1656.
- (23) de Dood, M. J. A.; Polman, A.; Fleming, J. G. *Phys. Rev. B* **2003**, *67*, 115106.
- (24) Vos, W. L.; Megens, M.; van Kats, C. M.; Bösecke, P. *J. Phys.: Condens. Matter* **1996**, *8*, 9503.
- (25) Galisteo-López, J.; Palacios-Lidon, E.; Castillo-Martinez, E.; Lopez, C. *Phys. Rev. B* **2003**, *68*, 115109.
- (26) Koenderink, A. F.; Megens, M.; van Soest, G.; Vos, W. L.; Lagendijk, A. *Phys. Lett. A* **2000**, *268*, 104.
- (27) Spry, R. J.; Kosan, D. J. *Appl. Spectrosc.* **1986**, *40*, 782.
- (28) Koenderink, A. F.; Vos, W. L. *Phys. Rev. Lett.* **2003**, *91*, 213902.
- (29) Galstyan, A. G.; Raikh, M. E.; Vardeny, Z. V. *Phys. Rev. B* **2000**, *62*, 1780.
- (30) James, R. W. *The Optical Principles of the Diffraction of X-Rays*; Ox Bow Press: Woodbridge, CT, 1962.
- (31) Vos, W. L.; van Driel, H. M. *Phys. Lett. A* **2000**, *272*, 101.
- (32) Wijnhoven, J. E. G. J.; Vos, W. L. *Science* **1998**, *281*, 802.
- (33) Wijnhoven, J. E. G. J.; Bechger, L.; Vos, W. L. *Chem. Mater.* **2001**, *13*, 4486.
- (34) Bechger, L. *Synthesis and Fluorescence of Opal and Air-Sphere Photonic Crystals*. Ph.D. Thesis, University of Twente, 2003.
- (35) The Γ -L notation results from the Brillouin zone, where Γ and L correspond to symmetry points (0, 0, 0) and (1/2, 1/2, 1/2), respectively.
- (36) Band structure calculations were done by Femius Koenderink with the use of a model where a volume fraction of 74% and 11% of the high index material and a refractive index of 1.59 and 1.76 for polystyrene opals and alumina inverse opals was assumed respectively.³⁷
- (37) Koenderink, A. F. *Emission and Transport of Light in Photonic Crystals*. Ph.D. Thesis, University of Amsterdam, 2003.
- (38) Galisteo-López, J. F.; López, C. *Phys. Rev. B* **2004**, *70*, 035108.
- (39) Míguez, H.; Kitaev, V.; Ozin, G. A. *Appl. Phys. Lett.* **2004**, *84*, 1239.
- (40) Flück, E.; van Hulst, N. F.; Vos, W. L.; Kuipers, L. *Phys. Rev. E* **2003**, *68*, 015601.
- (41) Labilloy, D.; Benisty, H.; Weisbuch, C.; Krauss, T. F.; Cassagne, D.; Jouanin, C.; Houdre, R.; Oesterle, U.; Bardinal, V. *IEEE J. Quantum Electron.* **1999**, *35*, 1045.